ELSEVIER

Surface Science 394 (1997) 105–118

surface science

Gas-source growth of group IV semiconductors: III. Nucleation and growth of Ge/Si(001)

I. Goldfarb *, J.H.G. Owen, P.T. Hayden, D.R. Bowler, K. Miki, G.A.D. Briggs

University of Oxford, Department of Materials, Parks Road, Oxford, OX1 3PH, UK

Received 28 March 1997; accepted for publication 30 July 1997

Abstract

The growth of Ge on Si(001) using gas-source molecular beam epitaxy (GSMBE) from GeH_4, has been investigated in situ, by elevated-temperature scanning tunnelling microscopy. While Si grows epitaxially in the Frank–van der Merwe mode, Ge grows heteroepitaxially in the Stranski–Krastanow mode. Nevertheless, at low coverages and/or low temperatures, comparison with Si growth from Si_2H_6 yields similar behaviour. At coverages less than one monolayer, the epitaxial strain is low enough to allow for such an Si-like growth, and at temperatures below 600 K neither Ge nor Si can grow properly due to hydrogen blockage of surface diffusion. The growth can be roughly divided into three different regimes, $T<600$ K (H-induced roughening), $600<T<700$ K (island-nucleation mode), and $T>700$ K (step-flow mode), where the gas flux is the second important growth parameter since, together with the temperature, it determines the diffusion length. At coverages higher than one monolayer, Ge growth no longer resembles that of Si, and a series of complex Ge/Si(001) phase transitions takes place. At $600<T<700$ K the sequence of phase transitions is as follows: $(2\times1)\Rightarrow(2\times N)\Rightarrow(M\times N)\Rightarrow$"hut" clusters. Growth at $T>700$ K changes the sequence to $(2\times1)\Rightarrow(2\times N)\Rightarrow(M\times N)\Rightarrow$"hut" pits$\Rightarrow$"hut" clusters. In this regime the wetting layer (8–9 ML) is significantly thicker than in the analogous solid-state MBE regime (3–4 ML). This difference can be attributed to the surfactant role of hydrogen present on the surface in the GSMBE process. A detailed Ge/Si(001) growth diagram, covering the temperatures mentioned above, is presented.

Keywords: Epitaxy; Germanium; Growth; Scanning tunnelling microscopy; Silicon ; Surface roughening

1. Introduction

Si–Ge alloys and Si/Ge superlattices are attractive for semiconductor devices because of their compatibility with the existing Si-based technology. Ge on Si is a model system for the Stranski–Krastanow (S–K) growth mode, where the initial two-dimensional (2D) wetting layer grows pseudomorphically until the strain due to the 4.2% of lattice mismatch is eventually relaxed via formation of three-dimensional (3D) macroislands [1–3], or ripples [4,5]. $Si_{1-x}Ge_x$/Si exhibits a growth behaviour which varies from that of pure Si/Si ($x=0$) to that of pure Ge/Si ($x=1$). The misfit strain can also be relieved by misfit dislocations [6]. Strained SiGe layers can be used as a base for high-speed heterobipolar transistors, whereas dislocation-relaxed layers can be used for other devices [6]. The 3D roughness is, however, undesirable for any kind of planar device, although this does not mitigate against use for devices based on low-dimensional quantum structures [7–9]. For

* Corresponding author. Fax: (+44) 1865 273783; e-mail: ilan.goldfarb@materials.ox.ac.uk

0039-6028/97/$17.00
PII S0039-6028(97)00634-1

either purpose, full understanding of the roughening transition during heteroepitaxy is essential.

We dedicated our previous studies to detailed and separate investigations of the gas-source molecular beam epitaxy (GSMBE) processes of Ge/Si(001) and Si/Si(001), using in situ elevated-temperature scanning tunnelling microscopy (ET-STM) [10–14]. Hydrogen presence in GSMBE is known to reduce undesired effects, such as Ge segregation and Si–Ge intermixing [15,16]. To further reduce these effects, low growth temperatures (<750 K) were used. The aim of these experiments was to obtain a deeper understanding of the GSMBE growth mechanisms of Si and Ge, and this work summarises the comparison. Mo and Lagally [17,18] were the first to show that in the low-coverage limit the MBE growth of Ge is very similar to the Si growth. However, the presence of hydrogen on the surface is known to have a profound effect not only as a diffusion blocker [14,19], but also as a possible surfactant, which can bind to island and step edges [14], promoting various instabilities [20] and different scaling laws [21]. A fundamental understanding of the GSMBE processes of Ge and Si growth will prepare the background for our next task of studying the growth of $Si_{1-x}Ge_x$/Si alloys and superlattices.

2. Experimental

The Si wafers used for this study were n-doped 0.1 Ω cm, cut into 1×7 mm^2 pieces and chemically degreased ex vacuo. The samples were handled with ceramic tweezers and clamped to the Ta support on the holder by Ta clamps. In UHV, the samples were degassed for several hours, repeatedly flashed at 1400 K, quenched below 800 K and slowly cooled to the desired temperature. During the sample flashes and anneals, the pressure was kept below 10^{-7} Pa. Such treatment has generally proved effective in producing well-ordered (2×1) Si surfaces. Sample heating was achieved by passing a direct current through it. Temperatures were measured by an optical pyrometer with an accuracy of 30 K. Polycrystalline 0.3 mm W wires were electrochemically etched in 2 M NaOH solution to produce atomically sharp tips.

A Jeol ET-STM, equipped with low-energy electron diffraction (LEED/Auger) and reflection high-energy electron diffraction (RHEED), and capable of operation up to 1200°C was used. The base pressure of the STM chamber prior to growth was 1×10^{-8} Pa. Growth movies were taken during the exposure to germane and disilane (separately) at the growth temperatures and in "constant current" or "log I" mode, using currents around 0.1 nA and voltages between ± 3 V. GeH_4 and Si_2H_6 (both 99.99%) were fed separately through a precision needle-valve onto the sample mounted in the STM stage. In the multiple exposure mode, the tip was retracted while dosing for a short time, and put back to scan after the pressure reached its peak. In the continuous growth mode the tip was allowed to scan while a desired constant pressure was maintained. In our studies disilane (Si_2H_6) is preferred over silane (SiH_4), mainly because of the lower temperature at which it decomposes on the substrate. Temperatures from room-temperature (RT) to 720 K, and gas pressures in the 10^{-7}–10^{-5} Pa range, were used for growth. The coverage was determined by computerised subtraction of images from one another, after fixing the same fiducial points in each successive pair of images.

3. Results and discussion

3.1. Dosing by multiple exposures

The difference between MBE and GSMBE growth is demonstrated by a simple experiment of depositing Si or Ge onto Si(001) at RT, and comparing with the same surface after RT adsorption of Si_2H_6 or GeH_4. Whereas in MBE small ordered Si islands are formed even at RT, implying sufficient surface diffusion to sustain the (2×1)-ordered surface [22], in GSMBE the lack of surface diffusion and the activation for hydride decomposition cause a completely disordered surface to appear, when saturating coverages of Si_2H_6 are adsorbed [23,24]. Fig. 1a–c shows an Si(001) surface after exposure to GeH_4 at RT and subsequent annealing at 500 K, and Fig. 1d shows the same surface after a four times higher exposure, but this

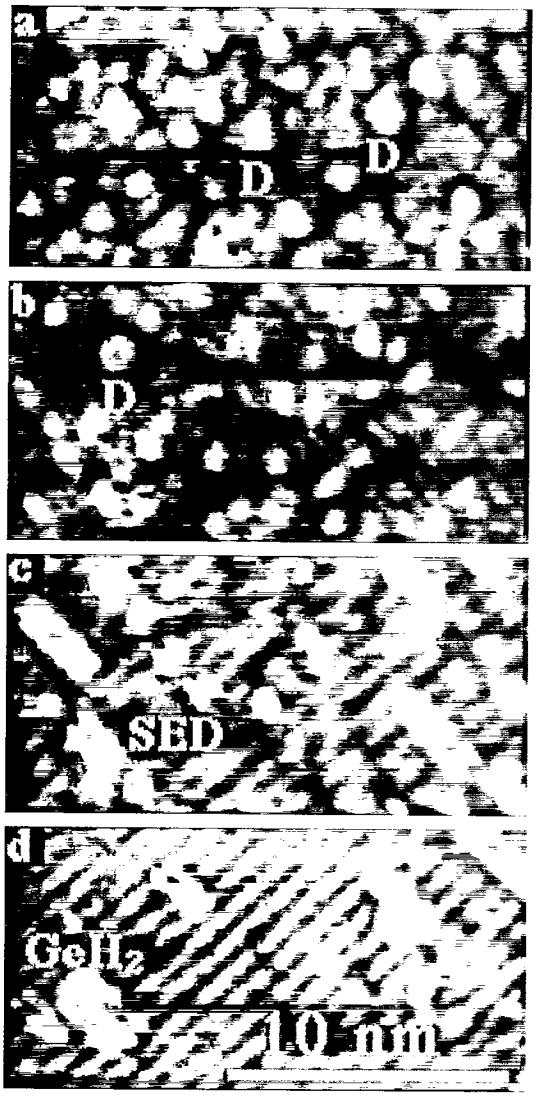

Fig. 1. Typical STM images of Si(001) surface at various stages of anneal after 0.04 L (Langmuir) RT exposure to GeH_4. "D" stands for "doughnut-like" and "SED" for "single epitaxial dimer". (a) Filled-states image at the beginning of anneal at 500 K, (b) after 25 min of anneal, (c) empty-states image after 40 min anneal, and (d) empty-states image after 0.16 L exposure at 520 K.

time at an elevated temperature of 520 K. Using the identification scheme for Si_2H_6 fragments proposed by Wang et al. [24], and making parallels with the SiH_4 decomposition scheme proposed by Gates and coworkers [25,26], various GeH_4 fragments, such as GeH_2, as well as single epitaxial dimers (SEDs) can be identified on the surface. As the annealing time progresses, the surface orders and SEDs (forming dimer strings) gradually replace the GeH_4 fragments, implying diffusion-controlled growth. Despite the apparent similarities between the RT adsorption followed by subsequent anneal (Fig. 1c) and the adsorption at the temperature similar to the annealing temperature (Fig. 1d), bearing in mind the significantly higher adsorbed dose and smaller island aspect-ratio in the latter case, one can conclude that to achieve some practical growth rate in a continuous deposition process, elevated substrate temperatures are a necessity.

These results are entirely consistent with our Si_2H_6 exposure experiments, including the "doughnut-like" features, marked "D" [13]. The very characteristic change from a "doughnut-like" appearance in the filled-states image (Fig. 1a,b) to a square appearance in the empty-states image (Fig. 2), is also completely consistent with our Si_2H_6 results, suggesting that the nucleation process proposed for the Si growth from Si_2H_6 [12] may also be valid for Ge growth from GeH_4. To confirm that this structure is stable for Ge as well as for Si, we have performed tight binding calculations of the clean Si surface, a Ge dimer in the epitaxial position on top of dimer row and a Ge square. We find that the Ge square is 1.43 eV more stable than two isolated Ge dimers. This can be compared with our tight binding and LDA calculations for the Si square [13], which implies that this

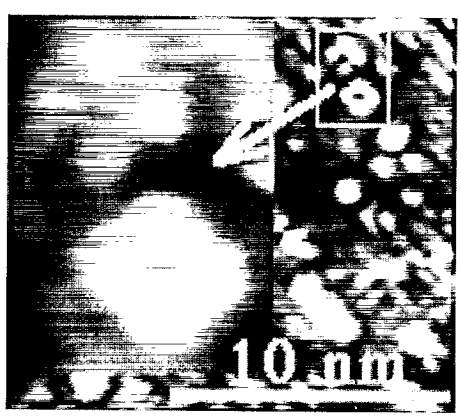

Fig. 2. Empty-states image of the Si(001) surface exposed to 0.12 L of GeH_4 at 470 K, in the course of a 570 K anneal.

feature is indeed more stable than isolated dimers and may well be a nucleus for dimer string growth. Fig. 3a shows a typical Si(001) surface after exposure to GeH_4, while Fig. 3b shows an Si(001) surface exposed to Si_2H_6 under roughly similar conditions.

Thus, summarising this subsection, the inevitable conclusion from our comparative studies of the initial stages of GSMBE growth of Ge and Si on Si(001) is that similar surface reaction pathways, and subsequent nucleation and growth mechanisms, must be active in both cases.

Fig. 3. Typical empty-states STM image of Si(001) surface after short exposures to GeH_4 and Si_2H_6 at elevated temperatures. (a) 0.24 L of GeH_4 at 540 K and (b) 0.27 L of Si_2H_6 at 610 K.

3.2. Continuous growth

The similarity between Ge and Si GSMBE growth in the low-coverage limit arises because in this limit there are no significant differences between S–K and Frank–van der Merwe growth modes. Therefore, as the Ge growth continues and the coverage increases, a progressive deviation from the 2D layer-by-layer growth is to be expected. In this subsection we will show how the deposition conditions, in particular substrate temperature, change the Ge growth. Again, where relevant, comparison with Si growth will be made.

3.2.1. Growth at $T > 700$ K

Fig. 4 shows Si growth in the relatively high-temperature ($T = 710$ K) regime. In this regime the surface diffusion is fast enough to accommodate rather high deposition pressures, or equivalently high arrival rates of the Si_2H_6 molecules. The effective diffusion length/terrace width ratio in this case is sufficiently high to allow for step-flow growth, rather than island-nucleation. The highly activated diffusants join the step-edges, promoting their advancement, e.g. "L" and "R" segments of the S_B step, while small islands, such as the one marked "I1" in Fig. 4a, even if they occasionally nucleate, cannot survive (see the absence of "I1" in Fig. 4b–d). (S_B steps, being perpendicular to the up-terrace dimer-rows, are better sinks for the ad-atoms, which preferentially diffuse along the dimer-rows, than S_A steps, which are parallel to the up-terrace dimer-rows [18].) The only types of island with a high probability of growing are the ones nucleating on antiphase boundaries (APBs), such as the one marked "I2", growing on a type-B APB (marked APB_B, where subscript "B" designates orientation relative to dimer-rows, analogous to designation of step-edges). B-type APBs were previously shown by other groups to play the role of nucleation centres, promoting multilayered growth (e.g. see Ref. [27]). Results of our atomistic modelling of APBs account for an increased stability of islands nucleated on APBs [14].

The same tendency to adsorb at the Si-substrate

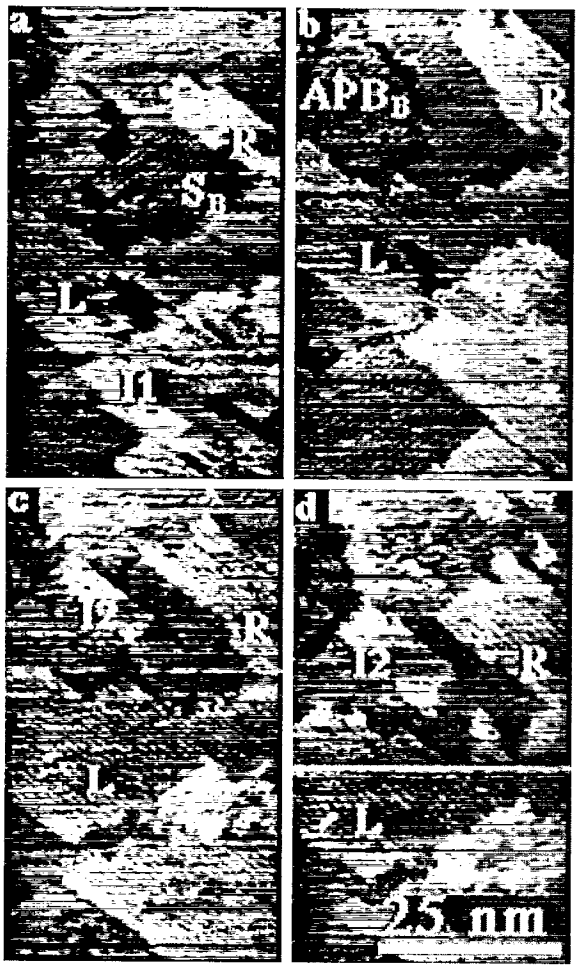

Fig. 4. A sequence from the empty-states STM movie, capturing Si growth from Si_2H_6. $T=710$ K, $P=5\times10^{-6}$ Pa.

S_B-steps is also observed during Ge/Si(001) growth; however, owing to the lower H-desorption temperatures in the presence of Ge [28] much higher deposition pressures can be sustained. Therefore, under the same temperature conditions (700 K), but a significantly higher pressure (1×10^{-5} Pa), the Ge/Si(001) growth regime shown in Fig. 5 is the same as the Si/Si(001) regime shown in Fig. 4 (710 K, 5×10^{-6} Pa). Fig. 5b shows the same region shown in Fig. 5a, but after deposition of about 0.7 monolayers of Ge ($\Theta\approx0.7$ ML). The kink, almost indistinguishable from the rest of the S_B step in Fig. 5a, has substantially advanced in Fig. 5b, where the direction and magnitude of the advancement are indicated by an arrow. At $\Theta\approx0.8$ ML we observed equally rough S_B and S_A steps, in excellent agreement with findings of Wu et al. [29], who were the first to document this phenomenon and the subsequent complete roughness-reversal. Wu et al. [29] attributed the reversal of relative roughness of the two types of step to a modification of kink energetics, introduced by dimer-vacancy lines (DVLs) of the Ge($2\times N$)/Si(2×1) reconstructed surface. The defect density starts to increase with Ge coverage in Fig. 5b, with progressive defect line-up in Fig. 5c–e. However, the step roughness is already completely reversed in Fig. 5d ($\Theta\approx1.1$ ML), whereas the $(2\times1)\Rightarrow(2\times N)$ transition leading to a fully ordered $(2\times N)$ reconstruction (giving visible superstructure satellites in a Fourier transform) does not appear before $\Theta\approx1.5$ ML. With further Ge deposition, the periodicity of N (distance between the DVLs) is progressively reduced, as can be deduced from Fig. 6a.

The next transition (Fig. 5g) begins at $\Theta\approx5$ ML, and is known as the $(2\times N)\Rightarrow$ "patched" structure transition [30]. Köhler et al. [31] suggested that, since filling the DVLs in the first Ge layer increases the strain, the second Ge layer will fill every second DVL, leaving every other DVL in the previous layer open, which leads to an appearance of a 2D rectangular mesh with $(N\times2N)$ periodicity. This argument is inconsistent with the three following observations: (a) in Fig. 7 we can see $(2\times N)$-reconstructed islands on a $(2\times N)$-reconstructed surface, i.e. all of the DVLs in the underlying layer are filled; (b) the width of the second type of vacancy line (VL) is larger, at least by a factor of two; (c) as can be seen in the arrowed locations in Fig. 5g,h, the second type of VL is often formed by agglomeration of defects in the uppermost layer before the next layer is deposited onto it.

Based on these observations, we propose a different model for the so-called "patched structure". The $(2\times1)\Rightarrow(2\times N)$ transition occurs because the second-layer atoms within each DVL rebond, giving rise to a large tensile stress along the topmost layer dimer-rows, which in turn partially cancels the compressive mismatch stress, thus lowering the overall elastic energy [32]. Thus the

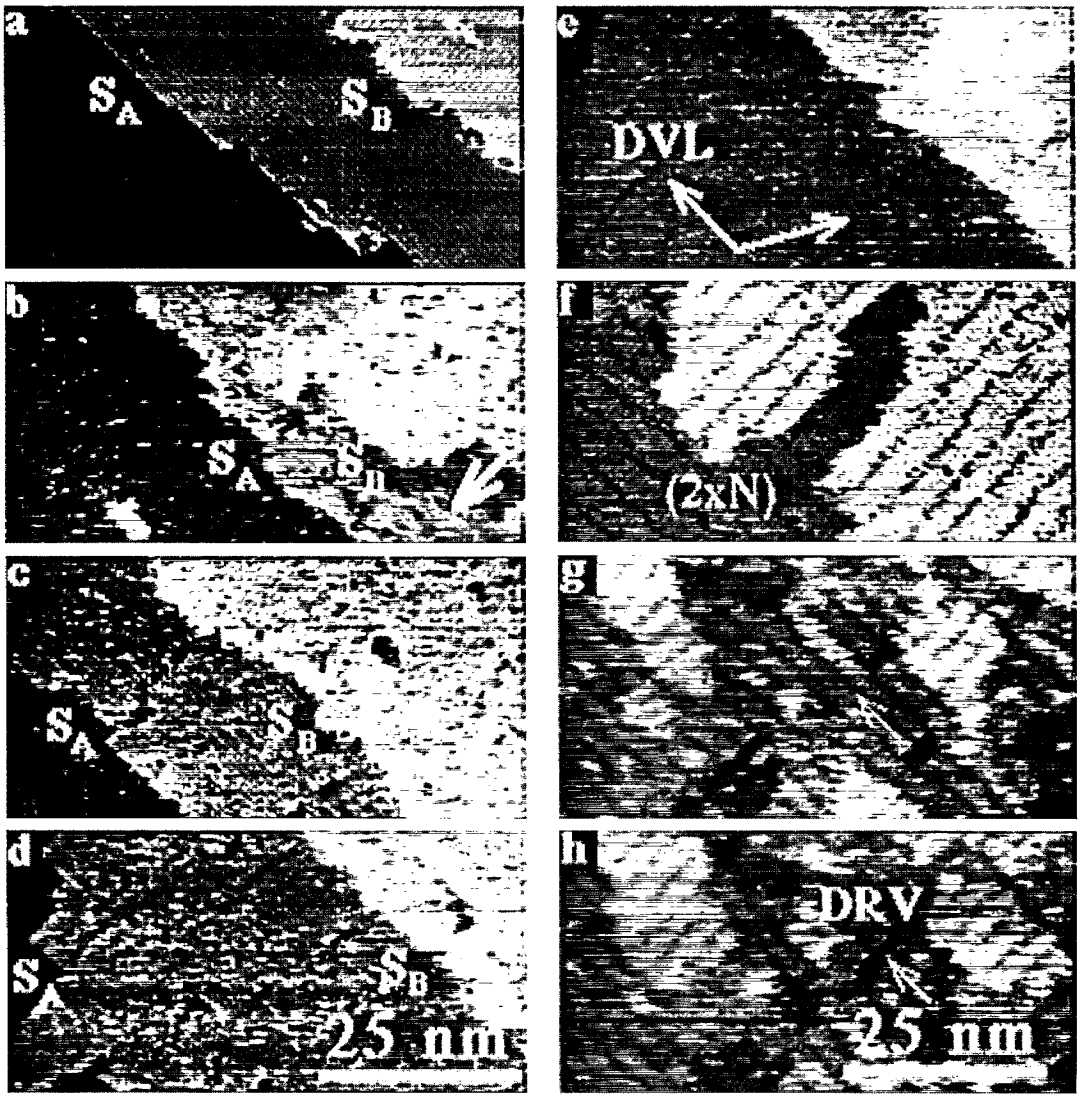

Fig. 5. A sequence from the STM movie, capturing Ge growth from GeH_4. $T=700$ K, $P=1\times10^{-5}$ Pa. (a)–(o) empty-states images, (p) filled-states image. (a) $\Theta=0$ ML, (b) $\Theta=0.7$ ML, (c) $\Theta=0.8$ ML, (d) $\Theta=1.1$ ML, (e) $\Theta=1.3$ ML, (f) $\Theta=3$ ML, (g) $\Theta=4.9$ ML, (h) $\Theta=5$ ML, (i) $\Theta=7.7$ ML, (j) $\Theta=7.9$ ML, (k) $\Theta=8.3$ ML, (l) $\Theta=8.4$ ML, (m) $\Theta=8.5$ ML; (n)–(p) show the progression of surface coverage by "hut" clusters. "V": voids; "P": pits; "C": clusters.

periodicity of the DVLs decreases with increasing Ge coverage, in order to continue to relieve the evolving stress. However, owing to short-range repulsive interaction between the DVs on the same dimer-row, the N-separation cannot decrease indefinitely. When the Ge-coverage exceeds the value corresponding to a minimal equilibrium N-separation (e.g. Fig. 5g), the stress cannot be further relieved by additional DVLs. This moment can be spotted by observing the ultimate straightening of the DVLs. The next possible stress-relaxation can be achieved by forming another set of VLs, but this time in the form of dimer-row vacancies (DRVs). Hereafter we will refer to their periodicity as the "M-periodicity". This explanation accounts for the formation of DRVs in

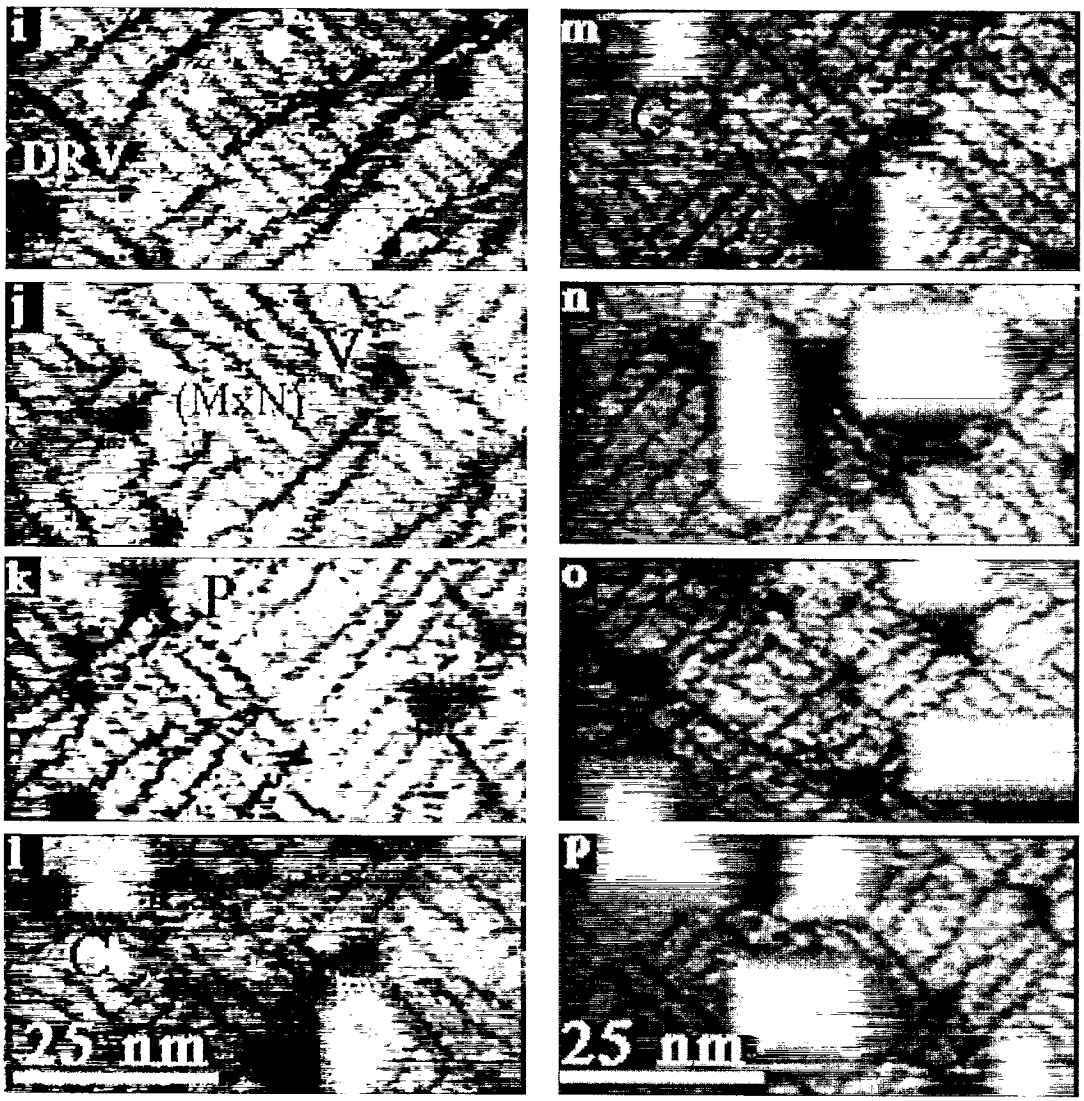

Fig. 5. (*continued*)

Fig. 5g,h, as well as for their increased width relative to a_0 in the case of DVLs (where $a_0 = 3.84$ Å is the Si surface lattice constant). The intersection between the previously formed DVLs and the subsequent DRVs, creates a 2D rectangular $(M \times N)$ grid on the surface (Fig. 5i). Thus, it is probably more correct to designate this transition as "$(2 \times N) \Rightarrow (M \times N)$", as opposed to "$(2 \times N) \Rightarrow$ patch". The fast decrease of M-separation with coverage (see Fig. 6) implies that DRVs are less efficient in relieving strain than DVLs, whereas the larger minimum spacing between DRVs is indicative of a stronger short-range repulsive interaction than between DVLs.

Fig. 5j shows the moment when the separation between DRVs reaches its minimal equilibrium spacing, indicated by ultimately straight DRVs (analogous to the previously reached minimal equilibrium spacing between DVLs); this signals the beginning of the 2D⇒3D growth transition. At 700 K this takes the form of an $(M \times N) \Rightarrow$"hut" pits transition, shown in Fig. 5k. The present

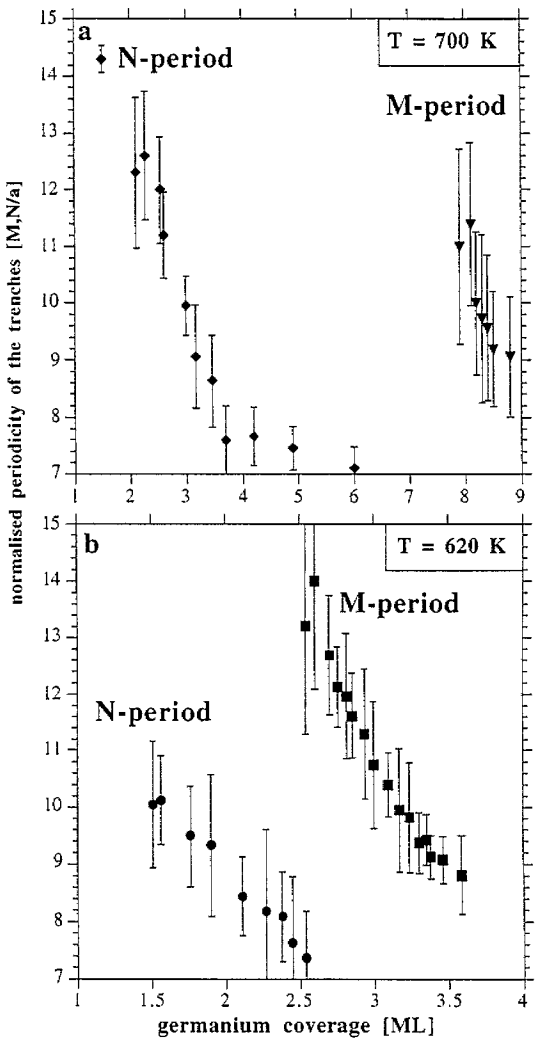

Fig. 6. The coverage-dependent behaviour of DVLs and DRVs at 620 K and 700 K. The bars represent the standard deviation of the mean.

authors were the first to observe this transition, as well as details of the nucleation mechanism for both "hut" pits and "hut" clusters [10]. When more Ge is deposited, the "hut" pits are replaced by "hut" clusters [10], as seen in Fig. 5l–p.

3.2.2. Growth at 600 < 700 K

In this regime both Si and, initially, Ge grow in the island-nucleation mode, as can be seen from comparison of Fig. 8 with Fig. 9a,b respectively (2D islands denoted as "I"). Details of Si growth

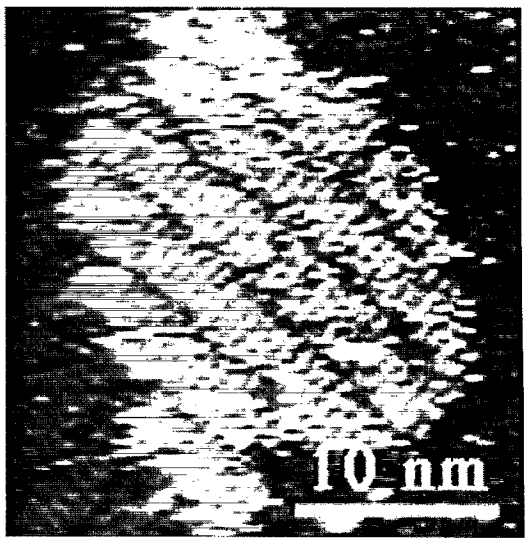

Fig. 7. Evidence for the ability of $(2\times N)$-layers to cover the underlying $(2\times N)$-reconstructed surface.

in this and other regimes are described elsewhere [14]. However, whereas Si grows in the fashion shown in Fig. 8 independent of the deposited thickness, Ge growth proceeds in general accordance with the scheme derived at 700 K, starting from $\Theta \approx 1$ ML (Fig. 9c), where the defects begin to line-up into DVLs. The two basic differences between Ge growth at 700 K and 620 K are that at the lower temperature the beginning of each transition is shifted to lower values of Θ, and, since the wetting layer is thinner, "hut" pits do not appear at all. The role of the wetting layer thickness in determining whether "hut" pits or "hut" clusters will follow the $(M\times N)$ reconstruction is described in a previous paper [10].

3.2.3. Growth at T < 600 K

Fig. 10 shows the progression of Si growth in the same regime as that observed for Ge growth below 600 K (Fig. 11). The growth temperature is the same as that shown in Fig. 8, i.e. 620 K; however, the Si_2H_6 pressure here is about 6×10^{-7} Pa, i.e. double that in Fig. 8, which brings it into the same regime as for Ge growth < 600 K. There is a dramatic change from a reasonable layer-by-layer growth in Fig. 8 to a situation where growth is impossible due to complete H-blockage

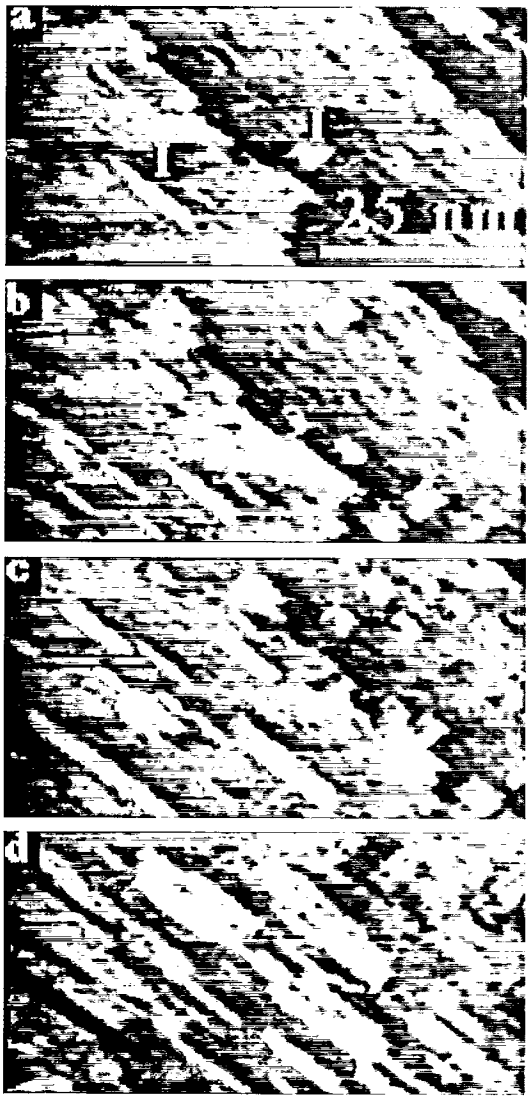

Fig. 8. Si growth from Si_2H_6 at $T=620$ K and $P=3\times10^{-7}$ Pa (filled-states image).

of Si diffusion pathways, shown in Fig. 10. The progressive blackening observed when going from Fig. 10a to Fig. 10e is only due to increasing concentration of hydrogen, since Si growth (unlike Ge growth) does not involve an increase in defect density with coverage (cf. Fig. 8).

On the other hand, a reasonable growth can be sustained in the case of Ge deposition at the same temperature with GeH_4 pressures as high as 1×10^{-5} Pa (see Fig. 9). This is due to a shift of hydrogen desorption temperatures to lower values in the presence of Ge on the surface: germanium lowers the activation barrier for recombinative desorption for both silicon mono- and dihydrides [32]. All our attempts to grow Ge at $T<600$ K have failed, even with GeH_4 pressures in the 10^{-7} Pa range. An example of such an attempt, at $T=570$ K is shown in Fig. 11, and the growth pattern seems to be identical to the blocked Si growth in Fig. 10. The minimum 600 K temperature for Ge growth may be closely related to the single hydrogen desorption temperature from the Ge surfaces, which is also 600 K [32].

3.3. Comparison with MBE

There are several important differences between the MBE growth of Si and Ge and the corresponding GSMBE growth from disilane and germane. These differences are perhaps best understood from the kinetic theory of gases. The deposition rate of atoms from the vapour phase is

$$R\,[\text{atoms cm}^{-2}\,\text{s}^{-1}] = \frac{3.51\times10^{22}\ \text{cm}^{-2}\times P\,[\text{Torr}]}{\sqrt{T\,[\text{K}]\times M.W.}} \times s\times n\,[\text{atoms/molecule}] \qquad (1)$$

where P is the deposition pressure, T is the gas temperature, $M.W.$ is the atomic/molecular weight, s is the sticking coefficient and n is the number of relevant atoms in the molecule, i.e. Ge atoms in GeH_4 and Si atoms in Si_2H_6. It is thus immediately clear that since the sticking coefficients of elemental Si and Ge are roughly similar, under identical pressure and temperature conditions the Si flux will only be higher than that of Ge by 60% due to its lower atomic weight. Taking into account the similar adsorption and diffusion properties explains the similarity in MBE growth rates for elemental Si and Ge [17,18,33].

Our measurements of growth rates show the sticking coefficient of GeH_4 to be about 0.065, whereas that of Si_2H_6 to be about 0.18, i.e. $s_{Si_2H_6}/s_{GeH_4}\approx3$! The difference due to different molecular weights (78 and 62 for GeH_4 and Si_2H_6 respectively) is negligible; however, each

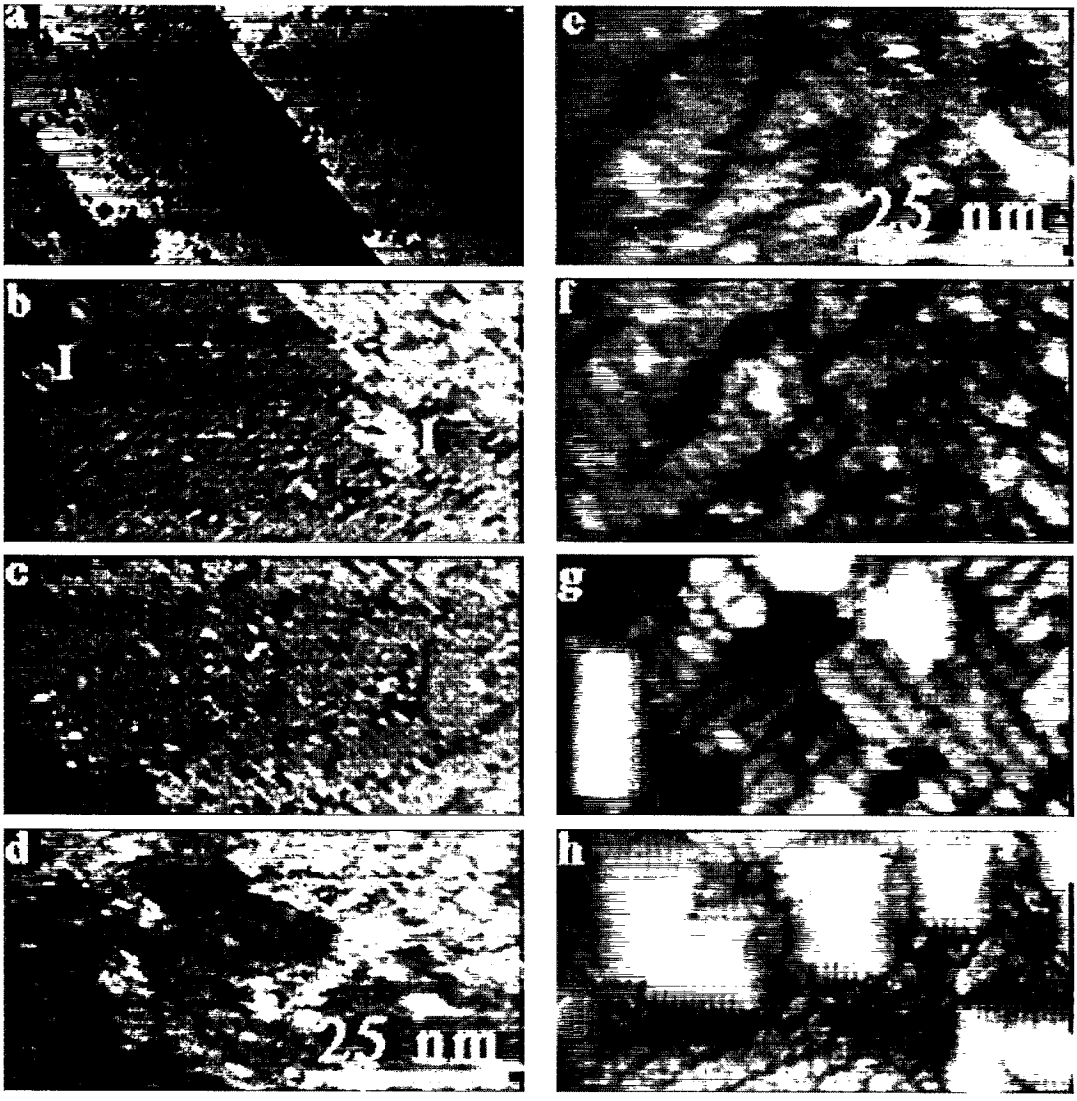

Fig. 9. Ge growth from GeH_4 at $T=620$ K and $P=5\times10^{-5}$ Pa. (a)–(g) filled-states image, (h) empty-states image. (a) $\Theta=0$ ML, (b) $\Theta=0.2$ ML, (c) $\Theta=1$ ML, (d) $\Theta=1.5$ ML, (e) $\Theta=2.5$ ML, (f) $\Theta=2.6$ ML, (g) $\Theta=3.5$ ML, (h) fully-grown "hut" clusters.

Si_2H_6 molecule contains two Si atoms, whereas each GeH_4 molecule contains only one Ge atom, which results in deposition rate of Si from Si_2H_6 six times higher than that of Ge from GeH_4 under identical deposition conditions. This result is rather important for growth of Si_xGe_{1-x} alloys. Fortunately, owing to the lower hydrogen desorption temperature from Ge-covered surfaces [32], higher Ge-growth rates can be achieved simply by increasing the GeH_4 pressure (without chocking the surface), since the rate is directly proportional to the pressure (see Eq. (1)). For example, comparison of the growth rate from Si_2H_6 in Fig. 4 (4×10^{-4} nm s^{-1} at 710 K and 5×10^{-6} Pa) to the growth rate from GeH_4 in Fig. 5 (1.4×10^{-4} nm s^{-1} at 700 K and 1×10^{-5} Pa) shows the Ge growth rate to be smaller than that of Si by a factor of less than three. Using the formula given above, we would expect there to be three times as many Si atoms arriving per second

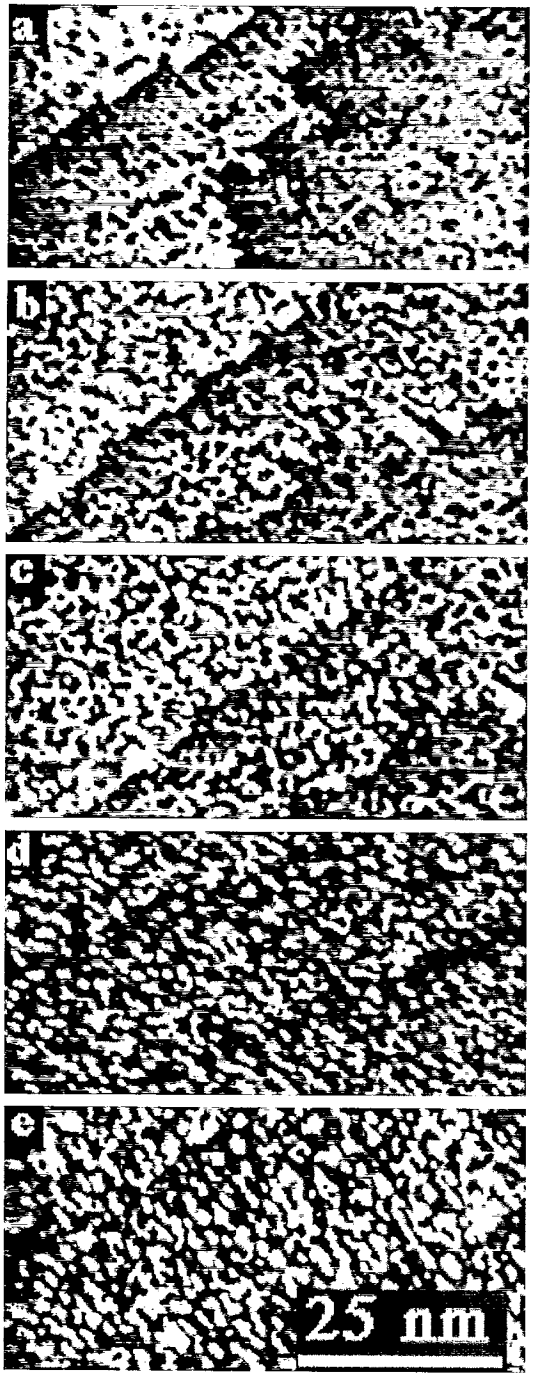

Fig. 10. Si growth from Si_2H_6 at $T=620$ K and $P=6\times10^{-7}$ Pa (filled-states image).

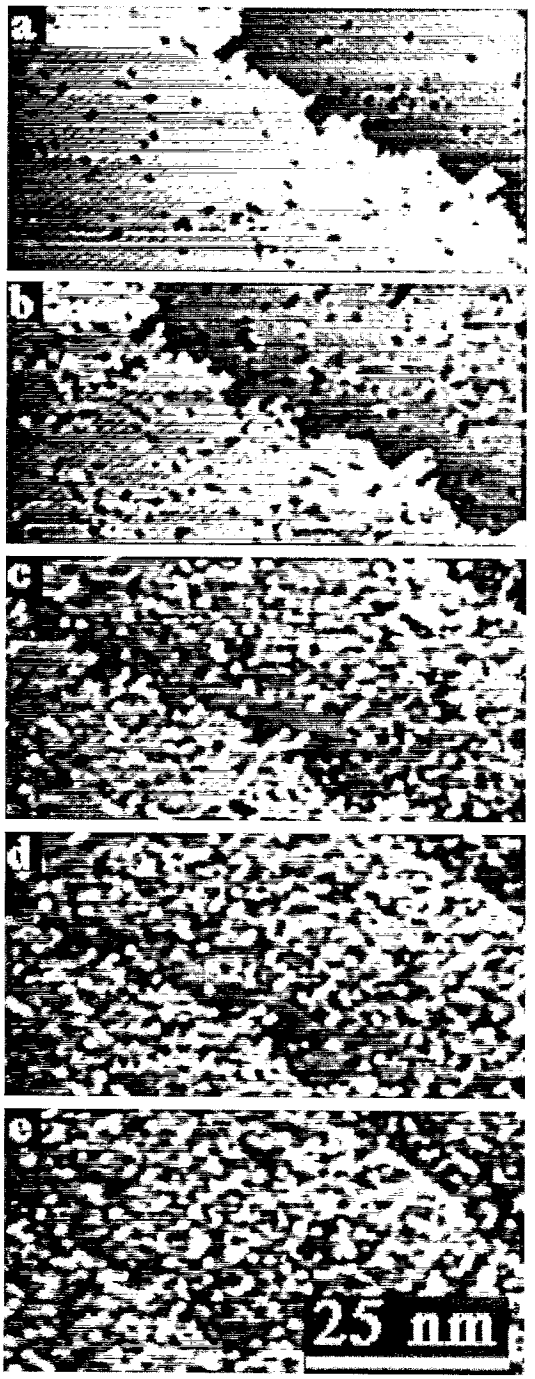

Fig. 11. Ge growth from GeH_4 at $T=560$ K and $P=1\times10^{-6}$ Pa (filled-states image).

as Ge, which is in good agreement with the different growth rates. The substrate temperature is sufficiently high that the hydrogen on the surface is not affecting the growth [12,14], and the lower desorption temperature for hydrogen from a Ge-covered surface will offset the higher number of H atoms per Ge atom. Under these conditions the ratio of diffusion lengths to terrace widths for both the Si- and Ge-grown surfaces (Figs. 4 and 5) causes them to be in the step-flow regime.

This is perhaps the place to compare GSMBE growth rates with those of typical MBE. Our GSMBE rates (in the order of 10^{-4} nm s^{-1}) are smaller by one order of magnitude than even the slowest MBE rates (in the order of 10^{-3} nm s^{-1}) [34], and by more than two orders of magnitude than the typical MBE rates [35,36]. One of the reasons for this is the lower deposition temperatures used in our study and, therefore, due to the blocking effect of hydrogen on the surface, smaller deposition pressures. The hydrogen acts as a diffusion-blocker at lower temperatures (Figs. 10–12) but as a surfactant at high enough temperatures due to sufficient thermal energy to activate floating properties. We expect that H-coverage at the monohydride level would produce surfactant behaviour similar to that of group V elements [20]. Our highest growth temperatures were high

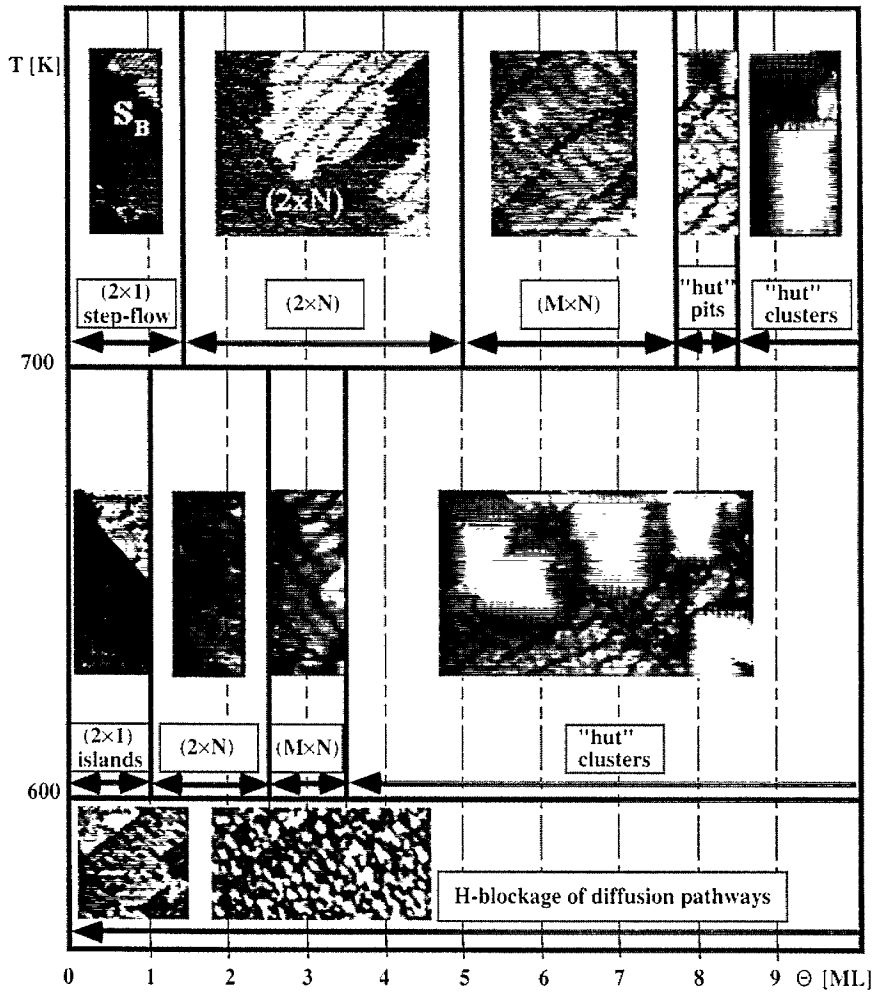

Fig. 12. A diagram describing the main stages of Ge/Si(001) growth from GeH_4, at $10^{-6} < P < 5 \times 10^{-5}$ Pa.

enough to activate the floating, but, nevertheless, were lower than the hydrogen β_1 desorption temperature even from the Ge-covered surface [28], leading to 2D growth.

4. Conclusions

Ge/Si(001) GSMBE growth from GeH_4 was investigated and compared with Si/Si(001) growth from Si_2H_6. The presence of the four-atom square structures in the Ge-grown surface implies that the Ge nucleation mechanism is identical to that proposed in our previous work for Si GSMBE growth [12].

The results of our study of Ge/Si(001) growth are best presented in a growth diagram with coverage–temperature coordinates, as shown in Fig. 12. This diagram differs from that previously proposed for solid-source MBE deposited Ge/Si(001) by Tomitori et al. [30]. This is mainly due to the characteristics inherent to the GSMBE process, such as H-blocked regions, and the thicker 2D wetting layer at high temperatures (see Fig. 12), which allows the formation of pits. The immediate implication is that, perhaps due to a surfactant action of hydrogen, in the GSMBE process at high temperatures a wetting layer thick enough (8–9 ML of Ge) to support "hut" pits can be grown. Such thick layers are not observed in the MBE Ge/Si(001) growth, where even at temperatures around 800 K the wetting layer thickness is in the order of 3–4 ML [30]. The surfactant role of hydrogen has also been seen by other investigators [37].

Close similarity was found between Si and Ge growth in the low-coverage limit, as well as in the low-temperature limit. In the low-coverage limit (less than 1 ML), the mismatch strain is low enough to allow for 2D island growth and to sustain the (2×1) surface reconstruction, similar to what was seen in the MBE-grown structures, whereas in the low-temperature limit ($T<600$ K) the growth of both Ge and Si is impeded by insufficiently mobile hydrogen. At temperatures around 700 K the growth mode of both Ge and Si changes from island-growth to step-growth.

Continuous growth reveals key differences, since the Ge/Si (unlike Si/Si) grows in an S–K mode, and when the coverage exceeds 1 ML a series of complex surface phase transitions eventually leads to 3D growth. The growth of both Ge and Si can be roughly divided into three regimes: at $T<600$ K the growth is choked by the excess of insufficiently mobile hydrogen; at $600<T<700$ K the initial growth is in the island-nucleation mode; $T>700$ K the growth proceeds initially in the step-flow mode.

Acknowledgements

We would like to thank M. Fearn, C.M. Goringe and D.G. Pettifor for fruitful discussions. This work is supported by EPSRC (GR/K08161). Computing facilities were provided by the Materials Modelling Laboratory, Oxford, which is partially funded by SERC Grant No. GR/H58278. J.H.G.O. and D.R.B are funded by the EPSRC. J.H.G.O. is partially funded by AEA Technology.

References

[1] D.J. Eaglesham, M. Cerullo, Phys. Rev. Lett. 64 (1990) 1943.
[2] D.J. Eaglesham, M. Cerullo, Mater. Sci. Eng. B 30 (1995) 197.
[3] M. Hammar, F.K. LeGoues, J. Tersoff, M.C. Reuter, R.M. Tromp, Surf. Sci. 349 (1995) 129.
[4] A.J. Cullis, D.J. Robbins, A.J. Pidduck, P.W. Smith, J. Cryst. Growth 123 (1992) 333.
[5] A.J. Pidduck, D.J. Robbins, A.J. Cullis, W.Y. Leong, A.M. Pitt, Thin Solid Films 222 (1992) 78.
[6] F.K. LeGoues, MRS Bull. 21 (4) (1996) 38.
[7] L. Banyai, S.W. Koch, Semiconductor Quantum Dots, World Scientific, Singapore, 1993.
[8] R. Nötzel, Semicond. Sci. Technol. 11 (1996) 1365.
[9] P.M. Petroff, G. Medeiros-Ribeiro, MRS Bull. 21 (4) (1996) 50.
[10] I. Goldfarb, P.T. Hayden, J.H.G. Owen, G.A.D. Briggs, Phys. Rev. Lett. 78 (1997) 3959.
[11] I. Goldfarb, P.T. Hayden, J.H.G. Owen, G.A.D. Briggs, Phys. Rev. B. in press.
[12] J.H.G. Owen, K. Miki, D.R. Bowler, C.M. Goringe, I. Goldfarb, G.A.D. Briggs, Surf. Sci. 394 (1997) this issue.
[13] J.H.G. Owen, D.R. Bowler, C.M. Goringe, K. Miki, G.A.D. Briggs, Surf. Sci. 382 (1997) L678.
[14] J.H.G. Owen, K. Miki, D.R. Bowler, C.M. Goringe, I. Goldfarb, G.A.D. Briggs, Surf. Sci. 394 (1997) this issue.

[15] G. Ohta, S. Fukatsu, Y. Ebuchi, T. Hattori, N. Usami, Y. Shiraki, Appl. Phys. Lett. 65 (1994) 2975.
[16] G. Ohta, S. Fukatsu, N. Usami, Y. Shiraki, T. Hattori, J. Cryst. Growth. 157 (1995) 36.
[17] Y.-W. Mo, M.G. Lagally, Surf. Sci. 248 (1991) 313.
[18] Y.-W. Mo, M.G. Lagally, J. Cryst. Growth 111 (1991) 876.
[19] J.E. Vasek, Z. Zhang, C.T. Sailing, M.G. Lagally, Phys. Rev. B 51 (1995) 17208.
[20] E. Kaxiras, Surf. Rev. Lett. 3 (1996) 1295.
[21] D. Kandel, Phys. Rev. Lett. 78 (1997) 499.
[22] M.G. Lagally, R. Kariotis, B.S. Swartzentruber, Y.-W. Mo, Ultramicroscopy 31 (1989) 87.
[23] M.J. Bronikowski, Y. Wang, M.T. McEllistrem, D. Chen, R.J. Hamers, Surf. Sci. 298 (1993) 50.
[24] Y. Wang, M.J. Bronikowski, R.J. Hamers, Surf. Sci. 311 (1994) 64.
[25] S.M. Gates, C.M. Greenlief, D.B. Beach, J. Chem. Phys. 93 (1990) 7493.
[26] S.M. Gates, S.K. Kulkarni, Appl. Phys. Lett. 58 (1991) 2963.
[27] M.J. Bronikowski, Y. Wang, R.J. Hamers, Phys. Rev. B 48 (1993) 12361.
[28] B.M.H. Ning, J.E. Crowell, Surf. Sci. 295 (1993) 79.
[29] F. Wu, X. Chen, Z. Zhang, M.G. Lagally, Phys. Rev. Lett. 74 (1994) 574.
[30] M. Tomitori, K. Watanabe, M. Kobayashi, O. Nishikawa, Appl. Surf. Sci. 76–77 (1994) 322.
[31] U. Köhler, O. Jusko, B. Müller, M. Horn-von Hoegen, M. Pook, Ultramicroscopy 42–44 (1992) 832.
[32] X. Chen, F. Wu, Z. Zhang, M.G. Lagally, Phys. Rev. Lett. 73 (1994) 850.
[33] V. Milman, D.E. Jesson, S.J. Pennycook, M.C. Payne, M.H. He, I. Stich, Phys. Rev. B 50 (1994) 2663.
[34] P.W. Deelman, T. Thundat, L.J. Schowalter, Appl. Surf. Sci. 104–105 (1996) 510.
[35] K. Fujita, S. Fukatsu, H. Yaguchi, Y. Shiraki, R. Ito, Appl. Phys. Lett. 59 (1991) 2240.
[36] P.C. Zalm, G.F.A. van de Walle, D.J. Gravesteijn, A.A. van Gorkum, Appl. Phys. Lett. 55 (1989) 2520.
[37] N. Ohtani, S. Mokler, M.H. Xie, J. Zhang, B.A. Joyce, Jpn. J. Appl. Phys. 34 (1994) 2311.